Real-space pseudopotential method for first principles calculations of general periodic and partially periodic systems

Amir Natan, Ayelet Benjamini, Doron Naveh, and Leeor Kronik*
Department of Materials and Interfaces, Weizmann Institute of Science, Rehovoth 76100, Israel

Murilo L. Tiago,† Scott P. Beckman, and James R. Chelikowsky
Center for Computational Materials, Institute for Computational Engineering and Science, Departments of Physics and Chemical Engineering, University of Texas, Austin, Texas 78712, USA

(Received 24 May 2008; revised manuscript received 2 July 2008; published 12 August 2008)

We present a real-space method for electronic-structure calculations of systems with general full or partial periodicity. The method is based on the self-consistent solution of the Kohn-Sham equations, using first principles pseudopotentials, on a uniform three-dimensional non-Cartesian grid. Its efficacy derives from the introduction of a new generalized high-order finite-difference method that avoids the numerical evaluation of mixed derivative terms and results in a simple yet accurate finite difference operator. Our method is further extended to systems where periodicity is enforced only along some directions (e.g., surfaces), by setting up the correct electrostatic boundary conditions and by properly accounting for the ion-electron and ion-ion interactions. Our method enjoys the main advantages of real-space grid techniques over traditional plane-wave representations for density functional calculations, namely, improved scaling and easier implementation on parallel computers, as well as inherent immunity to spurious interactions brought about by artificial periodicity. We demonstrate its capabilities on bulk GaAs and Na for the fully periodic case and on a monolayer of Si-adsorbed polar nitrobenzene molecules for the partially periodic case.

DOI: 10.1103/PhysRevB.78.075109 PACS number(s): 71.20.−b, 73.20.−r

I. INTRODUCTION

Density functional theory (DFT) (Ref. 1) has long been recognized as a practical means for first principles calculations of systems with a sizable number of electrons.[2] For periodic systems, such calculations are typically performed using a plane-wave expansion (see, e.g., Refs. 3–5), which provides an objective basis set allowing a natural representation of the Bloch functions. Unfortunately, conventional plane-wave programs require extensive "global" communications and as such are not amenable to massive parallelization. This can hinder large-scale computation unless special measures are employed and optimal use of the architecture is carefully controlled, as in the recent work of Gygi *et al.*[6] Alternatively, one can utilize localized basis sets with periodic boundary conditions (see, e.g., Refs. 7–9). Methods that utilize intrinsic locality in the representation can, in principle, be amenable to massive parallelization.[10] However, such constructions can be quite involved and, worse, localized basis set computations may exhibit serious convergence issues, especially for intrinsically delocalized systems such as metals and small-gap semiconductors.

The real-space pseudopotential method, where the Kohn-Sham equations are solved on a real-space grid using a high-order finite difference expansion, is an attractive alternative to both plane waves and localized basis sets.[11–13] The "basis set" provided by the grid is both objective and localized by construction. The resulting Hamiltonian is highly sparse, allowing for trivial grid-spacing-determined convergence *and* effective space-domain parallelization.[11,14,15] Originally developed for confined systems,[11] this approach can be used for periodic structures as well, using a uniform (e.g., Ref. 16) or an adaptive (e.g., Refs. 17–19) grid or a multigrid (e.g., Ref. 20) approach.

Previous work has shown that a straightforward uniform-grid-based high-order finite difference approach,[11] together with the use of pseudopotentials[21] and of advanced algorithms for solving large-scale electronic-structure problems,[22] as implemented in the PARSEC package,[12] can be used successfully for electronic-structure computations with hundreds, thousands, and even tens of thousands of electrons. Importantly, this is achieved with either nonperiodic ("open") boundary conditions[23] or with an orthorhombic periodic unit cell,[24] while avoiding the complications associated with adaptive grids, notably the difficulties associated with constructing a sufficiently accurate yet Hermitian discretization of the Laplacian operator.[19]

Unfortunately, a Cartesian grid is generally incompatible with the periodicity of nonorthorhombic unit cells. Retaining the simplicity of a uniform grid then requires that the grid be nonorthogonal.[18] The evaluation of the Laplacian operator is then more difficult: A direct evaluation of the Laplacian along the grid directions using the appropriate coordinate transformation results in mixed derivative terms, requiring $O(N^2)$ neighbors rather than $O(N)$ neighbors, for an N^{th} order expansion, forcing a tradeoff between accuracy and applicability.[18] Alternatively, one can resort to Mehrstellen methods,[20,25,26] i.e., the use of finite difference expansions at several grid points around a grid point where evaluation of the Laplacian is desired. However, this comes at the cost of loss of generality (i.e., absence of universal expression for any nonorthogonal grid) and possibly loss of hermiticity as well.[20]

Two-dimensional (2D) nonorthorhombic periodic cells often arise in the context of surfaces and interfaces.[27] An additional disadvantage of the plane wave approach in this context is that it inherently imposes periodicity in all three

dimensions so that surfaces are usually studied using a "repeated slab" approach. However, for polar surfaces the periodicity of the potential imposed by the spurious boundary condition is incompatible with the long-range electrostatic potential of a dipolar sheet.[28] Many clever schemes for mitigating or correcting this problem have been suggested.[28–37] In real-space calculations (and also in localized basis set ones), the problem need not arise at all because periodic boundary conditions can be enforced in two dimensions with an open boundary condition in the third.[38]

In this article, we show that straightforward high-order finite-difference calculations can be performed efficaciously on a nonorthogonal grid. This is achieved via a high-order, 3D generalization of a 2D stencil suggested by Brandt and Diskin[39] in the context of sonic flow calculations, allowing for the construction of a simple Hermitian $O(N)$ discrete representation for the Laplacian operator on the nonorthogonal grid. Furthermore, we present a simple method for the implementation of an open boundary condition in one dimension together with an (orthogonal or nonorthogonal) periodic grid in the other two dimensions. Taken together, this provides a powerful real-space pseudopotential method for large-scale first principles calculations of systems with arbitrary full or partial periodicity. The method is illustrated with numerical results for several representative three-dimensional (3D) and two-dimensional (2D) periodic systems.

II. METHODOLOGY

A. The real-space pseudopotential-DFT method

Implementation of the real-space pseudopotential-DFT method on a discrete orthogonal grid using high-order finite differences has been discussed in detail elsewhere for both periodic and nonperiodic boundary conditions.[11–16] Here, we briefly summarize the details essential to understanding implementation on a nonorthogonal grid.

In the Kohn-Sham approach to density functional theory, the interacting electron problem is mapped into an effective one-electron problem in the form

$$\left\{-\frac{1}{2}\nabla^2 + V_{\text{ion}}(\vec{r}) + V_H[\rho(\vec{r})] + V_{XC}[\rho(\vec{r})]\right\}\psi_n(\vec{r}) = \varepsilon_n\psi_n(\vec{r}). \tag{1}$$

Atomic units are used throughout. In Eq. (1) ε_n and $\psi_n(\vec{r})$ are the n^{th} single-electron eigenvalue and eigenfunction, respectively; $\rho(r)=\Sigma_{\text{occupied}}|\psi_n(\vec{r})|^2$ is the electron density; $V_{\text{ion}}(\vec{r})$ is the ionic potential, $V_H[\rho(\vec{r})]$ is the Hartree (classical electron-electron) potential, and $V_{XC}[\rho(\vec{r})]$ is the exchange-correlation potential. The total energy is then given by:

$$E_{\text{tot}}[\rho] = T_s[\rho] + E_{\text{ion}}(\{R_a\},[\rho]) + E_H[\rho] + E_{XC}[\rho] + E_{\text{ion-ion}}(\{R_a\}), \tag{2}$$

where $\{R_a\}$ are the nuclear positions, $T_s[\rho]$ is the kinetic energy of the noninteracting electrons, $E_{\text{ion}}(\{R_a\},[\rho])$ is the ion-electron potential energy, $E_H[\rho]$ is the Hartree energy, $E_{\text{ion-ion}}(\{R_a\})$ is the ion-ion electrostatic energy (evaluated using the usual Ewald summation[40] for periodic structures), and $E_{XC}[\rho]$ is the exchange correlation energy (with V_{XC} given by the functional derivative of $E_{XC}[\rho]$ with respect to the density).

In the pseudopotential approximation, only valence electrons are treated explicitly. Core electrons are suppressed by replacing the true ionic potential with an effective "pseudopotential" that accounts for the effect of the core electrons. This approximation greatly facilitates grid-based calculation as it results in slowly varying smooth potentials and wave functions. Therefore, in the following we take $\rho(r)$ and $V_{\text{ion}}(\vec{r})$ to denote the valence electron density and the pseudopotential, respectively.

For V_{ion}, we employ nonlocal norm-conserving pseudopotentials cast in the Kleinman-Bylander form.[41] In this form, the pseudopotential due to a single atom, $\hat{V}^a_{\text{ion}}$, is expressed as the sum of a local term and a nonlocal term, such that

$$\hat{V}^a_{\text{ion}}\psi_n(\vec{r}) = V_{\text{loc}}(|\vec{r}_a|)\psi_n(\vec{r}) + \sum_{l,m} G^a_{n,lm}u_{lm}(\vec{r}_a)\Delta V_l(r_a), \tag{3}$$

where $\vec{r}_a=\vec{r}-\vec{R}_a$, $u_{lm}(\vec{r}_a)$ is the atomic pseudo-wave-function corresponding to the angular momentum numbers lm, and the projection coefficients $G^a_{n,lm}$ are given by:

$$G^a_{n,lm} = \frac{1}{\langle \Delta V^a_{lm}\rangle}\int u_{lm}(\vec{r}_a)\Delta V_l(r_a)\psi_n(\vec{r})d^3r, \tag{4}$$

with

$$\langle \Delta V^a_{lm}\rangle = \int u_{lm}(\vec{r}_a)\Delta V_l(r_a)u_{lm}(\vec{r}_a)d^3r. \tag{5}$$

The Kleinman-Bylander form is advantageous in real space because outside the pseudopotential core cutoff radius, r_c, $\Delta V_l(\vec{r}_a)=0$ and $V^a_{\text{loc}}(\vec{r}_a)=-Z_{ps}/|\vec{r}_a|$, where Z_{ps} is the atomic number of the pseudoion. This limited nonlocality means that the discrete representation of $V_{\text{ion}}(\vec{r})$ is sparse.[11,12] Additionally, it means that in periodic systems only the local pseudopotential has infinite periodic replicas, and that those replicas behave in the usual $\sim 1/r$ manner of the true ionic potential.

The Hartree term in Eq. (1) is readily evaluated by solving the Poisson equation, $\nabla^2 V_H(\vec{r})=-4\pi\rho(\vec{r})$. For explicitly density-dependent functionals the exchange-correlation potential is given by an analytical approximation. Thus, evaluation of the remaining potential terms poses no special difficulty and results in purely diagonal contributions to the Hamiltonian matrix.

For evaluating the kinetic energy term, the second derivatives are expanded by:[11,42]

$$\frac{\partial^2}{\partial x^2} = \sum_{-N}^{N}\frac{c_n}{h^2}\psi(x_i+nh,y_j,z_k) + O(h^{2N}), \tag{6}$$

where h is the grid spacing and c_n are the N^{th} order finite difference coefficients for the second derivative expansion. On an orthogonal grid, the Laplacian is simply the sum of the second order derivatives and the following expression for the kinetic energy is obtained:

$$-\frac{1}{2}\sum_{k=-N}^{N}\frac{c_k}{h^2}[\psi_n(x_i+kh,y_j,z_k)+\psi_n(x_i,y_j+kh,z_k)+\psi_n(x_i,y_j,z_k+kh)], \quad (7)$$

i.e., the finite difference expression for the kinetic energy is also sparse as it involves a modest number of points around the point at which the Laplacian is evaluated. As shown in Ref. 11, $N=6$ is sufficient for most practical problems. For three distinct coordinates, this means there are $3\cdot 2\cdot 6+1=37$ elements in the discrete sum.

B. Implementation on a periodic nonorthogonal grid

For a periodic lattice, any wave function can be expressed as $\psi_{\vec{k}}(\vec{r})=e^{i\vec{k}\cdot\vec{r}}u_{\vec{k}}(\vec{r})$, where $u_{\vec{k}}(\vec{r})$ is a function with the periodicity of the lattice. Solving Eq. (1) for such a function, per a given value of $\vec{k}$, can be performed in two possible ways: First, one can leave the equation as is and account for the $e^{i\vec{k}\cdot\vec{r}}$ term by setting the periodic boundary conditions to be $\psi_{\vec{k}}(\vec{r}+\vec{R})=e^{i\vec{k}\cdot\vec{R}}\psi_{\vec{k}}(\vec{r})$. Alternatively (and as, e.g., in Ref. 19), one can substitute $\psi_{\vec{k}}(\vec{r})=e^{i\vec{k}\vec{r}}u_{\vec{k}}(\vec{r})$ in the equation and solve for $u_{\vec{k}}(\vec{r})$ with the periodic boundary conditions $u_{\vec{k}}(\vec{r}+\vec{R})=u_{\vec{k}}(\vec{r})$. Here, we choose the latter approach, which yields

$$\left[-\frac{1}{2}(\nabla+i\vec{k})^2+V_{\text{ion}}(\vec{r})+V_H(\vec{r})+V_{xc}(\vec{r})\right]u_{n,\vec{k}}(\vec{r})=E_n u_{n,\vec{k}}(\vec{r}), \quad (8)$$

where the kinetic energy operator is

$$-\frac{1}{2}(\nabla+i\vec{k})^2=-\frac{1}{2}(\nabla^2+2i\vec{\nabla}\cdot\vec{k}-\|\vec{k}\|^2). \quad (9)$$

Note that Eqs. (3) and (4) are expressed in terms of $\psi_{n,\vec{k}}(\vec{r})$ and not $u_{n,\vec{k}}(\vec{r})$. If phrased in terms of $u_{n,\vec{k}}(\vec{r})$, a multiplicative $e^{i\vec{k}\cdot\vec{r}}$ term should be added inside the integral of Eq. (4) and a multiplicative $e^{-i\vec{k}\cdot\vec{r}}$ term should be added before the summation in Eq. (3).

Now, let $\vec{a}_1$, $\vec{a}_2$, and $\vec{a}_3$ be the lattice vectors for a general periodic structure. We define lattice coordinates, (u,v,w), by $\vec{R}\equiv x\hat{e}_1+y\hat{e}_2+z\hat{e}_3\equiv u\hat{u}+v\hat{v}+w\hat{w}$, where $\hat{e}_i$ are unit vectors along the canonical orthogonal axes and $\hat{u}$, $\hat{v}$, and $\hat{w}$ are unit vectors along the lattice vector directions, namely, $\hat{u}=\vec{a}_1/|\vec{a}_1|$, $\hat{v}=\vec{a}_2/|\vec{a}_2|$, and $\hat{w}=\vec{a}_3/|\vec{a}_3|$. In matrix notation

$$\vec{R}_{xyz}=A\vec{R}_{uvw};\quad \vec{R}_{uvw}=B\vec{R}_{xyz}, \quad (10)$$

where $A\equiv[\hat{u},\hat{v},\hat{w}]$ and $B=A^{-1}$.

To express Eq. (8) in terms of the lattice coordinates (u,v,w), we must calculate the effect of the coordinate transformation on each of its terms. The gradient transformation is easily shown to be $\vec{\nabla}_{xyz}=B^T\vec{\nabla}_{uvw}$ and the Laplacian transformation is then $\vec{\nabla}^T_{xyz}\vec{\nabla}_{xyz}=\vec{\nabla}^T_{uvw}BB^T\vec{\nabla}_{uvw}$. Defining $F\equiv BB^T$, we can now rewrite the kinetic energy operator of Eq. (9) as

$$-\frac{1}{2}(\nabla^2_{xyz}+2i\vec{\nabla}_{xyz}\cdot\vec{k}-\|\vec{k}\|^2)=-\frac{1}{2}[\nabla^T_{uvw}F\nabla_{uvw}+2i(B^T\vec{\nabla}_{uvw})\cdot\vec{k}-\|\vec{k}\|^2]. \quad (11)$$

With an appropriate modified expression for the Laplacian, the Hartree term can also be evaluated by solving the Poisson equation in lattice coordinates. The other two terms, namely the ionic and exchange-correlation potentials, pose no particular difficulty and can be evaluated as explained above as long as the proper metric of the nonorthogonal cell is taken in all pertinent integrals. Naively, it would thus seem that solving the Kohn-Sham equations on a nonorthogonal grid is no more difficult than solving it on an orthogonal one. However, because F is generally not diagonal, the kinetic energy term [Eq. (11)] now contains mixed second derivatives. Therefore (and as explained in Ref. 17), a direct attempt for a finite difference discretization of Eq. (11) will contain $O(N^2)$ terms in the summation because one needs to include off-diagonal neighboring points in a square of size $(2N+1)\times(2N+1)$ around any given point. For, e.g., $N=6$, this would imply 469 elements in the expression for the 3D Laplacian, as compared with 37 for the orthogonal grid. This has direct adverse consequences for computation time and interprocessor communication. The same problem would also affect the Hartree term via the Laplacian operator in the Poisson equation.

To solve this Laplacian calculation problem, we generalize to high-order finite differences in 3D, an idea used (in the theory of sonic flow) for 2D structures with low-order expansion.[39] In its most general form, we can express the 3D Laplacian in lattice coordinates as

$$\nabla^2=f_{uu}\frac{\partial^2}{\partial u^2}+f_{vv}\frac{\partial^2}{\partial v^2}+f_{ww}\frac{\partial^2}{\partial w^2}+f_{uv}\frac{\partial^2}{\partial u\,\partial v}+f_{uw}\frac{\partial^2}{\partial u\,\partial w}+f_{vw}\frac{\partial^2}{\partial v\,\partial w}, \quad (12)$$

where

$$f_{uu}=F_{11},\quad f_{vv}=F_{22},\quad f_{ww}=F_{33},\quad f_{uv}=F_{12}+F_{21},\quad f_{uw}=F_{13}+F_{31},\quad f_{vw}=F_{23}+F_{32}. \quad (13)$$

Consider a system which is non-Cartesian in 2D, i.e., $\hat{w}$ is orthogonal to the uv plane and hence $f_{uw}=f_{vw}=0$. We define a new normalized direction, shown in Fig. 1, as the sum or difference of the original normalized lattice vectors:[43]

$$\hat{\mu}^{\pm}_{uv}=(\hat{u}\pm\hat{v})/|\hat{u}\pm\hat{v}|. \quad (14)$$

By definition of a directional derivative, one finds[44]

$$\frac{\partial}{\partial\mu^{\pm}_{uv}}=\frac{1}{|\hat{u}\pm\hat{v}|}\left(\frac{\partial}{\partial u}\pm\frac{\partial}{\partial v}\right), \quad (15)$$

$$\frac{\partial^2}{\partial\mu^{\pm 2}_{uv}}=\frac{1}{|\hat{u}\pm\hat{v}|^2}\left(\frac{\partial^2}{\partial u^2}+\frac{\partial^2}{\partial v^2}\pm 2\frac{\partial^2}{\partial u\,\partial v}\right).$$

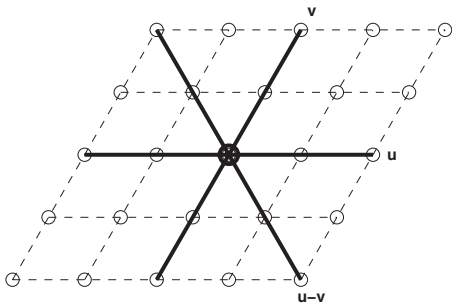

FIG. 1. Schematic representation of the $\hat{u}$, $\hat{v}$, and $\hat{u}-\hat{v}$ directions. Here the angle between $\hat{u}$ and $\hat{v}$ is acute so that $\hat{u}-\hat{v}$ is the preferred direction for derivation—see text for details.

Because the second directional derivative includes a mixed derivative term, we can use it together with Eq. (12) to eliminate the explicit appearance of the mixed derivative term $\partial^2/\partial u\,\partial v$. After some algebra, we obtain the following expression for the Laplacian:

$$\nabla^2 = (f_{uu} \mp f_{uv}/2)\frac{\partial^2}{\partial u^2} + (f_{vv} \mp f_{uv}/2)\frac{\partial^2}{\partial v^2} + f_{ww}\frac{\partial^2}{\partial w^2} \pm \frac{k_{uv}^{\pm}}{2}\frac{\partial^2}{\partial \mu_{uv}^{\pm 2}}, \tag{16}$$

where $k_{uv}^{\pm} = f_{uv}|\hat{u} \pm \hat{v}|^2$. In discrete form, this becomes

$$\nabla^2\psi(u_i,v_j,w_k) = \sum_{n=-N}^{N} c_n \left[\frac{f_{uu} \mp f_{uv}/2}{h^2}\psi(u_i+nh,v_j,w_k) + \frac{f_{vv} \mp f_{uv}/2}{h^2}\psi(u_i,v_j+nh,w_k) + \frac{f_{ww}}{h^2}\psi(u_i,v_j,w_k+nh) \pm \frac{k_{uv}^{\pm}}{2h_{uv}^2}\psi(u_i+nh,v_j \pm nh,w_k)\right] + O(h^{2N}), \tag{17}$$

where $h_{uv} \equiv h|\hat{u} \pm \hat{v}|$ is the grid spacing along the new direction.[45]

The choice between the "+" and "−" directions in Eqs. (14)–(17) is made so as to minimize the effective grid spacing along in the chosen direction, given by $h_{uv}^{\pm} = h\sqrt{2[1 \pm \cos(\theta)]}$, where θ is the angle between $\hat{u}$ and $\hat{v}$. If $\theta < \pi/2$, the chosen direction is the "−" one, whereas if $\theta > \pi/2$ the chosen direction is the '+' one. Figure 1 shows a simple illustration for the "'−" direction for the former case.

In the general, 3D non-Cartesian case, where $\hat{w}$ is not orthogonal to the uv plane, we have three mixed derivative terms. For their elimination, it makes sense to seek three additional directions, instead of one. It also stands to reason to seek directions with minimal grid spacing along the chosen directions, i.e., to choose the extra directions to point to the nearest neighbors on the grid. If we denote the unit vectors pointing in these three additional directions as $\hat{\mu}_i = \mu_{i1}\hat{u} + \mu_{i2}\hat{v} + \mu_{i3}\hat{w}$, by definition of a directional derivative, we obtain[44]

$$\frac{\partial}{\partial \mu_i} = \mu_{i1}\frac{\partial}{\partial u} + \mu_{i2}\frac{\partial}{\partial v} + \mu_{i3}\frac{\partial}{\partial w};$$

$$\frac{\partial^2}{\partial \mu_i^2} = \mu_{i1}^2\frac{\partial^2}{\partial u^2} + \mu_{i2}^2\frac{\partial^2}{\partial v^2} + \mu_{i3}^2\frac{\partial^2}{\partial w^2} + 2\mu_{i1}\mu_{i2}\frac{\partial^2}{\partial u\,\partial v} + 2\mu_{i1}\mu_{i3}\frac{\partial^2}{\partial u\,\partial w} + 2\mu_{i2}\mu_{i3}\frac{\partial^2}{\partial v\,\partial w}. \tag{18}$$

We now seek three coefficients, b_i, such that the mixed derivative part of Eq. (12), $f_{uv}\partial^2/\partial u\,\partial v + f_{uw}\partial^2/\partial u\,\partial w + f_{vw}\partial^2/\partial v\,\partial w$, is equal to $b_1\partial^2/\partial\mu_1^2 + b_2\partial^2/\partial\mu_2^2 + b_3\partial^2/\partial\mu_3^2$. Using Eq. (18), this leads to a trivial set of linear equations for b_i

$$2\begin{bmatrix} \mu_{11}\mu_{12} & \mu_{21}\mu_{22} & \mu_{31}\mu_{32} \\ \mu_{11}\mu_{13} & \mu_{21}\mu_{23} & \mu_{31}\mu_{33} \\ \mu_{12}\mu_{13} & \mu_{22}\mu_{23} & \mu_{32}\mu_{33} \end{bmatrix}\begin{bmatrix} b_1 \\ b_2 \\ b_3 \end{bmatrix} \equiv M\begin{bmatrix} b_1 \\ b_2 \\ b_3 \end{bmatrix} = \begin{bmatrix} f_{uv} \\ f_{uw} \\ f_{vw} \end{bmatrix}. \tag{19}$$

The resulting Laplacian is then

$$\nabla^2 = \left(f_{uu} - \sum_{k=1}^{3} b_k\mu_{k1}^2\right)\frac{\partial^2}{\partial u^2} + \left(f_{vv} - \sum_{k=1}^{3} b_k\mu_{k2}^2\right)\frac{\partial^2}{\partial v^2} + \left(f_{ww} - \sum_{k=1}^{3} b_k\mu_{k3}^2\right)\frac{\partial^2}{\partial w^2} + \sum_{k=1}^{3} b_k\frac{\partial^2}{\partial \mu_k^2} \tag{20}$$

with a discretization made obvious by comparison of Eqs. (16) and (17).

Equations (16) and (20) show that, at the modest cost of more finite difference directions, mixed derivatives are eliminated. This immediately results in a discrete expression based on $O(N)$ neighboring points instead of $O(N^2)$ as in the direct discretization. In the worst case, where all b_k are nonzero, and for $N=6$, we obtain 73 elements in the discrete sum, as compared to 37 for the orthogonal grid. This should be contrasted with 469 elements for the direct implementation of mixed derivatives. Furthermore, the discrete implementation of this Laplacian stencil is Hermitian by construction because the coefficients of the second derivative are symmetric in each of the directions. We note that for complete evaluation of the kinetic energy term in Eq. (11), we also need to implement the gradient part after the transformation. However, this is straightforward and introduces no additional computational complexity.

As explicit examples of our approach, consider the Laplacian expression obtained for the high-symmetry cases of hexagonal (2D), fcc, and bcc unit cells, the complete derivation of which is given in Appendix. Interestingly, all these Laplacian expressions, as well as the usual orthogonal-grid expression for the (and 3D) simple cubic cell, take a particularly simple form

TABLE I. Coefficient f, nearest-neighbor directions v_i, and their number N_V for the highly symmetric Laplacian expression of Eq. (21).

	N_v	f	v_i
Simple cubic (2D)	2	1	$\hat{x},\hat{y}$
Hexagonal (2D)	3	2/3	$\hat{u},\hat{v},\hat{u}-\hat{v}$
Simple cubic	3	1	$\hat{x},\hat{y},\hat{z}$
Bcc	4	3/4	$\hat{u},\hat{v},\hat{w},\hat{u}+\hat{v}+\hat{w}$
Fcc	6	1/2	$\hat{u},\hat{v},\hat{w},\hat{u}-\hat{v},\hat{u}-\hat{w},\hat{v}-\hat{w}$

$$\nabla^2 = f\sum_{i=1}^{N_V} \frac{\partial^2}{\partial v_i^2}, \tag{21}$$

where the coefficient f, the nearest-neighbor directions v_i and their number N_V are given in Table I.[46] Note, in particular, that fN_V is equal to the dimensionality, d, in all these cases. This result can be explained by symmetry considerations alone. First, because the Laplacian operator is rotation invariant, all nearest-neighbor directions must have the same coefficient. Second, if we operate the Laplacian on a function that is spherically symmetric, all second derivatives are the same and the Laplacian must be given by $fN_V\partial^2\psi/\partial r^2$, regardless of the coordinate system, i.e., fN_V=const. Because for a Cartesian grid $N_V=d$ and $f=1$, $fN_V=d$ throughout.

Finally, note that in Eq. (20) we have chosen to represent the Laplacian with a combination of derivatives along the three original u, v, and w directions and three *additional* nearest-neighbor directions. In most commonly encountered unit cells, the original u, v, and w directions would indeed be nearest-neighbor directions. However, for some cells, e.g., rhombohedral cells with a cell angle smaller than 30°, the six nearest-neighbor directions do not include u, v, and w, and one could construct an even more efficient Laplacian out of those six directions using the same principles given above.

C. 2D partial boundary conditions

We define a 2D periodic system as a system that is periodic in two directions (say x and y) but nonperiodic in the third direction (say z). Clearly, we must treat the nonperiodic direction as in finite systems, i.e., defining a domain outside which the wave function is zero, while employing periodic boundary conditions as above in the other two directions. For such 2D partially periodic systems the axis along the finite direction is orthogonal to the plane of periodicity by construction and therefore the Laplacian stencil of Eq. (17) is appropriate. For a complete solution of the Kohn-Sham equation for this partially periodic case, special attention needs to be paid to three issues, where the approach must differ from that of either the fully periodic case or the fully nonperiodic one: (1) setting the correct boundary conditions for the Poisson equation, (2) calculating the ionic potential, and (3) calculating the ion-ion term in the total energy.

To set the correct boundary conditions for the Poisson equation in the nonperiodic direction, we show a method based directly on the asymptotic behavior of the electrostatic potential for two-dimensional systems.[47] We note that there are other methods for obtaining the correct boundary conditions, including introducing a cutoff in the Fourier space of the 3D periodic problem,[19,30] a Green's function formalism in Fourier space,[37] and using the Ewald-Kornfeld method to compute the multipole expansion for a 2D periodic structure in real space.[38] We prefer our direct approach as it is physically transparent, easy to implement, and computationally efficient.

We represent the periodic part of a two-dimensional density at the $z=0$ plane as a sum of its Fourier components:

$$\rho(x,y) = \rho_{av} + \sum_{l,m}{}' \rho_{l,m} e^{i\vec{k}_{l,m}\cdot\vec{r}_{xy}}, \tag{22}$$

where $\rho_{av}=1/|S|\sum_{\text{cell}}\rho(x,y)$, S is the periodic cell area, $\vec{r}_{xy}=(x,y,0)$, and $\vec{k}_{l,m}=l\vec{b}_1+m\vec{b}_2$, where $\vec{b}_1$, $\vec{b}_2$ are the reciprocal 2D lattice vectors, and l, m are integers. The following expression is then readily obtained for the potential $V(x,y,z)$:[47]

$$V(x,y,z) = -2\pi\rho_{av}|z| + 2\pi\sum_{l,m}{}' \frac{\rho_{l,m}}{|k_{l,m}|} e^{i(\vec{k}_{l,m}\cdot\vec{r}_{xy})} e^{-|\vec{k}_{l,m}||z|}. \tag{23}$$

The electrostatic potential at a boundary point (x,y,z) is then obtained immediately by considering the complete partially periodic system as a finite set of periodic sheets located at the grid planes z_i and calculating the sum of their potentials. The result is

$$V(x,y,z) = \sum_i \left[-2\pi\rho_{av}(z_i)|z-z_i| + 2\pi\sum_{l,m}{}' \frac{\rho_{l,m}(z_i)}{|k_{l,m}|} e^{i(\vec{k}_{l,m}\cdot\vec{r}_{xy})} e^{-|\vec{k}_{l,m}||z-z_i|} \right] \tag{24}$$

This expression is computationally efficient because the l, m summation converges rapidly due to the exponential decay term. We found that taking $l,m=6$ is more than sufficient. In fact, in many cases even the average dipole term alone is already enough for getting a rather accurate solution.

For the ionic potential, we employ a method similar to that described by Rozzi *et al.*[30] As explained above [see discussion below Eq. (5)], we need to deal with a nontrivial summation only for the local component of the pseudopotential, whose form for $r>r_c$ is simply the bare coulomb potential of the pseudoion. To handle the summation, we separate the local pseudopotential of each atom into a long-range component, $V_+(\vec{r}_a)$, and a short-range component, $\Delta V(\vec{r}_a)$, by adding and subtracting the potential of a Gaussian positive charge density, $n_+(\vec{r}_a)=(\gamma_a/\pi)^{3/2}Z\exp(-\gamma_a^2|\vec{r}_a|^2)$, the potential of which is $V_+(\vec{r}_a)=-Z\,\text{erf}(\gamma_a|\vec{r}_a|)/|\vec{r}_a|$, where $\vec{r}_a=\vec{r}-\vec{R}_a$. As in Ref. 30, we define

$$V_{loc}(\vec{r}_a) \equiv \Delta V(\vec{r}_a) + V_+(\vec{r}_a), \tag{25}$$

where

$$\Delta V^{|\vec{r}|>r_c}(\vec{r}_a) = -\frac{Z}{|\vec{r}_a|}(1-\mathrm{erf}(\gamma_a|\vec{r}_a|))$$

and

$$\Delta V^{|\vec{r}|<r_c}(\vec{r}_a) = V_{\mathrm{loc}}^{|\vec{r}|<r_c}(\vec{r}_a) + \frac{Z}{|\vec{r}_a|}\mathrm{erf}(\gamma_a|\vec{r}_a|). \quad (26)$$

The overall local pseudopotential is then given by:

$$V_{\mathrm{ion}}^{\mathrm{loc}}(r) = \sum_a \sum_p V_{\mathrm{ion},a}^{\mathrm{loc}}(|\vec{r}_a - \vec{P}|)$$
$$= \sum_a \left[\sum_p \Delta V_a(|\vec{r}_a - \vec{P}|) + \sum_p V_{+,a}(|\vec{r}_a - \vec{P}|) \right], \quad (27)$$

where a goes over all atoms in the system and $\vec{P}$ goes over all lattice displacement vectors. We choose the constants γ_a such that $\Delta V_a(\vec{r}_a)$ is practically zero a few periodic cells away from the atom so we only need a finite sum for this term. To determine the sum of the $V_{+,a}(\vec{r}_a)$ terms, we solve the Poisson equation for the known Gaussian charges $n_{+,a}(r_a)$, with the appropriate boundary conditions as explained above.[48]

As for the Ewald summations, it is important to realize that the standard Ewald expressions for evaluating the ion-ion contribution to the total energy for 3D periodic structures[40] are not appropriate here. However, expressions appropriate for partial 2D periodicity have been given in the literature[38,49] so this poses no particular difficulty.

We note that the strategies proposed here for all three issues raised above, namely solution of the Poisson equation, evaluation of the ionic potential, and Ewald summation, are readily extended to partially periodic systems with only one periodic dimension. As this need not involve a nonorthogonal grid, this issue shall be pursued elsewhere.

III. RESULTS

In this section, we demonstrate the validity of the above presented formalism for both fully and partially periodic systems, with a nonorthogonal unit cell, as implemented in the PARSEC package.[12]

For fully periodic structures, we demonstrate our approach using bulk GaAs, a semiconductor with an fcc lattice, and bulk Na, a metal with a bcc lattice. We choose these examples because they often serve as benchmarks for plane-wave codes and therefore allow an easy assessment of the present approach. However, we have tested the methodology with cells of arbitrary symmetry, including monoclinic cells. The results are compared to standard plane wave calculations using the PARATEC code.[50] Importantly, the same pseudopotentials were used in both PARSEC and PARATEC, so that any residual differences may arise only from the numerical method used to solve the pseudopotential-Kohn-Sham equations and from the transcription of pseudopotentials between real and Fourier space.

Real-space results for the band structure of GaAs using the local density approximation (LDA) exchange-correlation functional with scalar-relativistic Troullier-Martins pseudopotentials[51] are shown in Fig. 2(a). $s/p/d$ cutoff radii (in atomic unit) of 1.80/2.20/2.80 (Ga) and 1.80/2.10/2.50 (As), with electronic configuration of $4s^2 4p^1 4d^0$ (Ga) and $4s^2 4p^3 4d^0$ (As), and nonlinear core correction radii (in atomic unit) of 1.0 (Ga) and 1.4 a.u. (As) were used. A $7\times7\times7$ k-point sampling scheme was used, with a 0.2 a.u grid spacing. PARATEC calculations are not shown because visually their results are indistinguishable from those given in Fig. 2(a). The total energy in the two calculations differed by only $\sim 10^{-5}$ Ry, clearly establishing the equivalence between the plane-wave and real-space calculations.[52] We attribute the residual differences to subtle differences in the sampling procedures of the pseudopotential onto a radial grid in both Fourier space and real space, and to the interpolation of the radial grid onto the computed plane-wave components or 3D grid points.

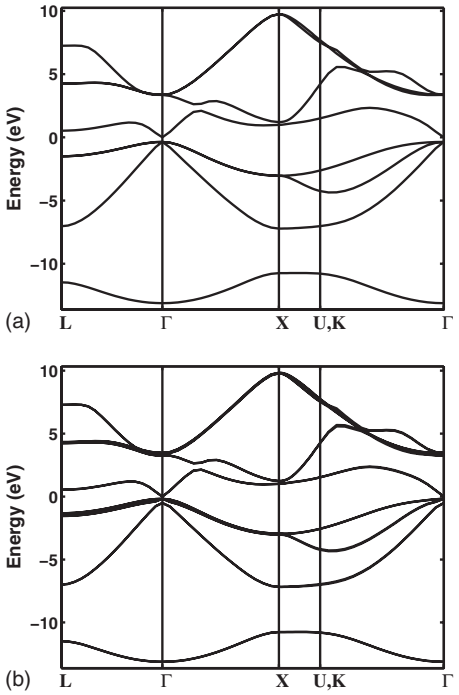

FIG. 2. Real-space calculation within the local density approximation for the band structure of GaAs along selected high-symmetry directions in the Brillouin zone, using (a) scalar-relativistic and (b) fully relativistic (i.e., including spin-orbit coupling) pseudopotentials.

Importantly, the formalism presented here is fully compatible with our recently reported real-space pseudopotential method for incorporating spin-orbit coupling effects.[53] By generating spin-orbit pseudopotentials,[53] using the same parameters as above and solving the ensuing spinor equations fully self-consistently, we obtained the GaAs relativistic band structures shown in Fig. 2(b). We cannot compare these results directly to the PARATEC ones as spin-orbit effects are not implemented in the PARATEC version at our disposal. However, Table II reveals an excellent agreement with previously reported results[54–56] for the energy levels at selected high-symmetry k points, and also agrees with reported spin-orbit splitting values,[57] again establishing the validity and accuracy of our approach.

TABLE II. A comparison of computed relativistic results, in eV, for the eigenvalue spectrum of GaAs at the three special points, Γ, *X*, and *L*. Full-potential Koringa-Kohn-Rostocker (FKKR), Ref. 54. Full-potential linearized augmented plane waves (FLAPW), Ref. 55. Plane waves and pseudopotentials (PWPP), Ref. 56. Real space and pseudopotentials (RSPP), this work.

Level	FKKR	FLAPW	PWPP	RSPP
Γ_6^v	−12.94	−12.91	−12.71	−12.95
Γ_7^v	−0.35	−0.34	−0.35	−0.34
Γ_8^v	0.00	0.00	0.00	0.00
Γ_6^c	0.12	0.17	0.60	0.17
Γ_7^c	3.46		3.40	3.42
Γ_8^c	3.66		3.60	3.64
X_6^v	−10.42	−10.41	−10.40	−10.59
X_7^v	−7.02	−7.00	−6.86	−7.00
X_6^v	−2.88	−2.85	−2.74	−2.85
X_7^v	−2.79	−2.76	−2.65	−2.77
X_6^c	1.17	1.23	1.21	1.18
X_7^c	1.39		1.42	1.41
L_6^v	−11.18	−11.14	−11.11	−11.30
L_6^v	−6.83	−6.82	−6.65	−6.82
L_6^v	−1.38	−1.36	−1.32	−1.37
$L_{4,5}^v$	−1.17	−1.16	−1.10	−1.15
L_6^c	0.71	0.73	0.92	0.72
L_6^c	4.38		4.34	4.42
$L_{4,5}^c$	4.46		4.44	4.50

Real-space results for the band structure of Na using LDA with a Troullier-Martins pseudopotential[51] are shown in Fig. 3. $s/p/d$ cutoff radii (in atomic unit) of 3.10/3.10/3.10, with electronic configuration of $3s^1 3p^0 3d^0$ and a nonlinear core

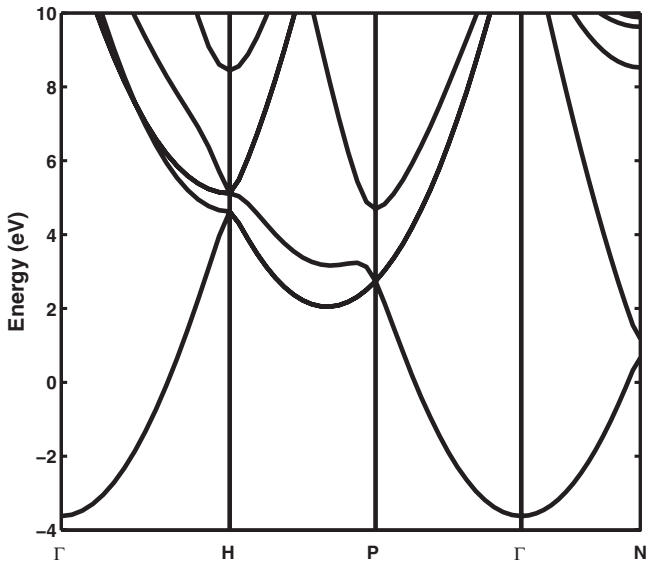

FIG. 3. Real-space calculation within the local density approximation for the band structure of Na along selected high-symmetry directions in the Brillouin zone. The Fermi energy has been chosen as the zero energy.

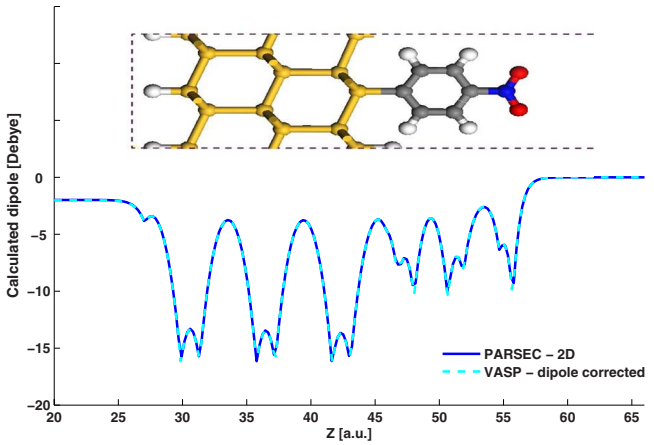

FIG. 4. (Color online) Electrostatic dipole per cell as a function of position, for a nitrobenzene monolayer adsorbed on the Si(111) surface, computed within a partially periodic PARSEC calculation and a fully periodic dipole-corrected VASP calculation. The unit cell structure is given above the dipole curves on the same scale.

correction radius (in atomic unit) of 1.0 were used. A $12 \times 12 \times 12$ *k*-point sampling scheme was used for Na, with a 0.3 a.u grid spacing. PARATEC calculations are again not shown because visually their results are indistinguishable from those given in Fig. 3. The total energy difference between PARATEC and PARSEC was $\sim 10^{-4}$ Ry.[52] The PARSEC and PARATEC results are also in excellent agreement with an independent calculation performed using the Vienna *ab initio* simulation package (VASP),[58] which is not shown for brevity. This clearly demonstrates that just like plane-wave calculations, our approach handles metallic and nonmetallic structures on the same footing.

We demonstrate the efficacy of our treatment for partially periodic systems by computing the electronic structure of a polar monolayer of nitrobenzene adsorbed on the Si (111) surface.[59] We chose this system as it possesses a significant dipole and because it has been shown that in the absence of any corrections, spurious 3D periodicity can cause gross errors in the evaluation of its polarity.[33] The dipole as a function of position has been computed from the charge density as prescribed in Refs. 33 and 59. A comparison of the dipole per cell, computed based on the partially periodic PARSEC calculation and a fully periodic dipole-corrected[28] calculation within VASP, is shown in Fig. 4. Both calculations were performed using the local density approximation, with periodic dimensions of 3.83 Å × 6.64 Å and a $3 \times 3 \times 1$ k-point sampling scheme. PARSEC calculations were performed using a 0.2 a.u. grid spacing using Troullier-Martins pseudopotentials[51] with $s/p/d$ or s/p cutoff radii (in atomic unit) of 2.5/ 2.5/2.5 (Si); 1.3/1.3 (C); 1.45/1.45 (O); 1.5/ 1.5 (N); 1.0/1.2/1.2 (H)—all generated from the neutral atom configuration. The dimension of the cell in the finite direction was 26.46 Å. The VASP calculations were performed with a 400-eV energy cutoff, with a dimension in the artificially periodic direction of 40 Å, and the dipole correction scheme of Ref. 28. It is readily observed that the two calculations are virtually identical on the scale of the plot. The overall difference between the two codes in the total dipole per cell across the entire structure is a small 0.027D, which

we attribute to the effect of different grid sampling and different pseudopotentials used.

IV. CONCLUSIONS

We presented a real-space method for electronic-structure calculations of systems with general full or partial periodicity. The method is based on the self-consistent solution of the Kohn-Sham equations, using first principles pseudopotentials, on a uniform three-dimensional non-Cartesian grid. Its efficiency derives from the introduction of a new generalized high-order finite-difference method that, by using additional differencing directions, avoids the numerical evaluation of mixed derivative terms and results in a simple yet accurate finite difference operator. We extended the method to systems where periodicity is enforced only along some directions by setting up the correct electrostatic boundary conditions and by properly accounting for the ion-electron and ion-ion interactions. Our method enjoys the main advantages of real-space grid techniques over traditional plane-wave representations for density functional calculations, namely, improved scaling and easier implementation on parallel computers, as well as inherent immunity to spurious interactions brought about by artificial periodicity. We demonstrated its capabilities on bulk GaAs and Na for the fully periodic case and for a monolayer of Si-adsorbed polar nitrobenzene molecules for the partially periodic case. For all cases, excellent agreement with plane wave codes was obtained.

ACKNOWLEDGMENTS

Work at the Weizmann Institute was partly supported by an Israel Science Foundation "Converging Technologies" grant. Three of us (M.L.T., S.P.B., and J.R.C.) acknowledge support by the National Science Foundation under Grant No. DMR-0551195 and the U.S. Department of Energy under Grants No. DE-FG02-06ER15760 and No. DE-FG02-06ER46286. D.N. and L.K. thank S. Sanvito (Trinity College Dublin) for kindly supplying Ga and As pseudopotential parameters.

APPENDIX: EXPLICIT LAPLACIAN EXPRESSION FOR HEXAGONAL, FCC, AND BCC CELLS

For a hexagonal lattice, the A matrix defined after Eq. (10) is

$$A=[\hat{u},\hat{v},\hat{w}]=\begin{bmatrix}1 & 1/2 & 0\\ 0 & \sqrt{3}/2 & 0\\ 0 & 0 & 1\end{bmatrix}. \tag{A1}$$

With the definition $B=A^{-1}$ we get

$$F=BB^{T}=\begin{bmatrix}4/3 & -2/3 & 0\\ -2/3 & 4/3 & 0\\ 0 & 0 & 1\end{bmatrix}, \tag{A2}$$

which yields the coefficients for the Laplacian of Eq. (12)

$$f_{uu}=f_{vv}=4/3;\quad f_{uv}=-4/3;\quad f_{uw}=f_{vw}=0;\quad f_{ww}=1. \tag{A3}$$

Using the additional nearest-neighbor direction $\hat{u}-\hat{v}$, Eq. (16) then yields

$$\nabla^2=\frac{2}{3}\frac{\partial^2}{\partial u^2}+\frac{2}{3}\frac{\partial^2}{\partial v^2}+\frac{\partial^2}{\partial w^2}+\frac{2}{3}\frac{\partial^2}{\partial \mu_{uv}^{-2}}, \tag{A4}$$

the discrete representation of which is

$$\nabla^2\psi(u_i,v_j,w_k)=\sum_{n=-N}^{N}\frac{c_n}{h^2}\left[\frac{2}{3}\psi(u_i+nh,v_j,w_j)+\frac{2}{3}\psi(u_i,v_j+nh,w_k)+\psi(u_i,v_j,w_k+nh)+\frac{2}{3}\psi(u_i+nh,v_j-nh,w_k)\right]+O(h^{2N}). \tag{A5}$$

For an fcc lattice, the A matrix defined after Eq. (10) is

$$A=[\hat{u},\hat{v},\hat{w}]=\begin{bmatrix}0 & 1/\sqrt{2} & 1/\sqrt{2}\\ 1/\sqrt{2} & 0 & 1/\sqrt{2}\\ 1/\sqrt{2} & 1/\sqrt{2} & 0\end{bmatrix}. \tag{A6}$$

With the definition $B=A^{-1}$ we get

$$F=BB^{T}=\begin{bmatrix}3/2 & -1/2 & -1/2\\ -1/2 & 3/2 & -1/2\\ -1/2 & -1/2 & 3/2\end{bmatrix}, \tag{A7}$$

which yields the coefficients for the Laplacian of Eq. (12)

$$f_{uu}=f_{vv}=f_{ww}=1.5,$$

$$f_{uv}=f_{uw}=f_{vw}=-1.0. \tag{A8}$$

In the fcc grid the additional nearest-neighbor directions are $\mu_1=\hat{u}-\hat{v}$, $\mu_2=\hat{u}-\hat{w}$, and $\mu_3=\hat{v}-\hat{w}$. This yields

$$\boldsymbol{\mu}=\begin{bmatrix}1 & -1 & 0\\ 1 & 0 & -1\\ 0 & 1 & -1\end{bmatrix}\Rightarrow M=\begin{bmatrix}-2 & 0 & 0\\ 0 & -2 & 0\\ 0 & 0 & -2\end{bmatrix}$$

$$\Rightarrow\begin{bmatrix}b_1\\ b_2\\ b_3\end{bmatrix}=-\frac{1}{2}\begin{bmatrix}f_{uv}\\ f_{uw}\\ f_{vw}\end{bmatrix}, \tag{A9}$$

where the elements μ_{ij} of the matrix $\boldsymbol{\mu}$ are given in Eq. (18), and M and b_i are given in Eq. (19). Substituting in Eq. (20), we get

$$\nabla^2=0.5\frac{\partial^2}{\partial u^2}+0.5\frac{\partial^2}{\partial v^2}+0.5\frac{\partial^2}{\partial w^2}+0.5\frac{\partial^2}{\partial \mu_1^2}+0.5\frac{\partial^2}{\partial \mu_2^2}+0.5\frac{\partial^2}{\partial \mu_3^2}, \tag{A10}$$

the discrete form of which is

$$\nabla^2\psi(u_i,v_j,w_k) = \frac{1}{2}\sum_{n=-N}^{N}\frac{c_n}{h^2}[\psi(u_i+nh,v_j,w_j) + \psi(u_i,v_j+nh,w_k) + \psi(u_i,v_j,w_k+nh) + \psi(u_i+nh,v_j-nh,w_k) + \psi(u_i+nh,v_j,w_k - nh) + \psi(u_i,v_j+nh,w_k-nh)] + O(h^{2N}). \quad \text{(A11)}$$

Similarly, for a bcc cell we have

$$A = [\hat{u},\hat{v},\hat{w}] = \frac{1}{\sqrt{3}}\begin{bmatrix} -1 & 1 & 1 \\ 1 & -1 & 1 \\ 1 & 1 & -1 \end{bmatrix}$$

$$\Rightarrow F = BB^T = \begin{bmatrix} 3/2 & 3/4 & 3/4 \\ 3/4 & 3/2 & 3/4 \\ 3/4 & 3/4 & 3/2 \end{bmatrix} \quad \text{(A12)}$$

and $f_{uu}=f_{vv}=f_{ww}=f_{uv}=f_{uw}=f_{vw}=1.5$.

For the bcc grid, the nearest-neighbor directions are $\hat{u}$, $\hat{v}$, $\hat{w}$, and $\hat{u}+\hat{v}+\hat{w}$. We choose two additional directions from among the second nearest neighbors $\hat{u}+\hat{v}$ and $\hat{u}+\hat{w}$. Using Eqs. (18) and (19) as above we find

$$\mu = \begin{bmatrix} 1 & 1 & 1 \\ \sqrt{3}/2 & \sqrt{3}/2 & 0 \\ \sqrt{3}/2 & 0 & \sqrt{3}/2 \end{bmatrix}$$

$$\Rightarrow M = 2\begin{bmatrix} 1 & 3/4 & 0 \\ 1 & 0 & 3/4 \\ 1 & 0 & 0 \end{bmatrix} \Rightarrow \begin{bmatrix} b_1 \\ b_2 \\ b_3 \end{bmatrix} = \begin{bmatrix} 3/4 \\ 0 \\ 0 \end{bmatrix}, \quad \text{(A13)}$$

i.e., the extra second-neighbor directions are in fact not needed. Using Eq. (20) we get

$$\nabla^2 = \frac{3}{4}\frac{\partial^2}{\partial u^2} + \frac{3}{4}\frac{\partial^2}{\partial v^2} + \frac{3}{4}\frac{\partial^2}{\partial w^2} + \frac{3}{4}\frac{\partial^2}{\partial \mu_1^2}, \quad \text{(A14)}$$

the discrete representation of which is

$$\nabla^2\psi(u_i,v_j,w_k) = \frac{3}{4}\sum_{n=-N}^{N}\frac{c_n}{h^2}[\psi(u_i+nh,v_j,w_j) + \psi(u_i,v_j+nh,w_k) + \psi(u_i,v_j,w_k+nh) + \psi(u_i+nh,v_j+nh,w_k+nh)] + O(h^{2N}). \quad \text{(A15)}$$

*leeor.kronik@weizmann.ac.il
†Present address: Materials Science and Technology Division, Oak Ridge National Laboratory, Oak Ridge, TN 37831.

[1] P. Hohenberg and W. Kohn, Phys. Rev. **136**, B864 (1964); W. Kohn and L. J. Sham, *ibid.* **140**, A1133 (1965).
[2] See, e.g., R. M. Martin, *Electronic Structure: Basic Theory and Practical Methods* (Cambridge University Press, Cambridge, 2004); W. Koch and M. C. Holthausen, *A Chemist's Guide to Density Functional Theory*, 2nd ed. (Wiley, Heidelberg, 2001).
[3] J. Ihm, A. Zunger, and M. L. Cohen, J. Phys. C **12**, 4409 (1979).
[4] M. D. Segall, P. J. D. Lindan, M. J. Probert, C. J. Pickard, P. J. Hasnip, S. J. Clark, and M. C. Payne, J. Phys.: Condens. Matter **14**, 2717 (2002).
[5] G. Kresse and J. Hafner, J. Phys.: Condens. Matter **6**, 8245 (1994).
[6] F. Gygi, E. W. Draeger, M. Schulz, B. R. de Supinski, J. A. Gunnelss, V. Austel, J. C. Sexton, F. Franchetti, S. Kral, C. W. Ueberhuber, and J. Lorenz, Proceedings of the 2006 ACM/IEEE Conference on Supercomputing, edited by B. Horne-Miller (ACM, New York, 2006).
[7] M. D. Towler, A. Zupan, and M. Caush, Comput. Phys. Commun. **98**, 181 (1996).
[8] D. Sánchez-portal, P. Ordejón, E. Artacho, and José M. Soler, Int. J. Quantum Chem. **65**, 453 (1997).
[9] K. N. Kudin and G. E. Scuseria, Chem. Phys. Lett. **289**, 611 (1998).
[10] C.-K. Skylaris, P. D. Haynes, A. A. Mostofi, and M. C. Payne, J. Chem. Phys. **122**, 084119 (2005).
[11] J. R. Chelikowsky, N. Troullier, and Y. Saad, Phys. Rev. Lett. **72**, 1240 (1994); J. R. Chelikowsky, N. Troullier, K. Wu, and Y. Saad, Phys. Rev. B **50**, 11355 (1994).
[12] L. Kronik, A. Makmal, M. L. Tiago, M. M. G. Alemany, M. Jain, X. Huang, Y. Saad, and J. R. Chelikowsky, Phys. Status Solidi B **243**, 1063 (2006).
[13] T. L. Beck, Rev. Mod. Phys. **72**, 1041 (2000).
[14] A. Stathopoulos, S. Öğüt, Y. Saad, J. R. Chelikowsky, and H. Kim, Comput. Sci. Eng. **2**, 19 (2000).
[15] J. R. Chelikowsky, A. T. Zayak, T.-L. Chan, M. L. Tiago, Y. Zhou, and Y. Saad, J. Phys.: Condens. Matter (to be published).
[16] M. M. G. Alemany, M. Jain, L. Kronik, and J. R. Chelikowsky, Phys. Rev. B **69**, 075101 (2004).
[17] F. Gygi and G. Galli, Phys. Rev. B **52**, R2229 (1995).
[18] N. A. Modine, G. Zumbach, and E. Kaxiras, Phys. Rev. B **55**, 10289 (1997); U. V. Waghmare, H. Kim, I. J. Park, N. Modine, P. Maragakis, and E. Kaxiras, Comput. Phys. Commun. **137**, 341 (2001).
[19] A. Castro, H. Appel, M. Oliveira, C. A. Rozzi, X. Andrade, F. Lorenzen, M. A. L. Marques, E. K. U. Gross, and A. Rubio, Phys. Status Solidi B **243**, 2465 (2006).
[20] E. L. Briggs, D. J. Sullivan, and J. Bernholc, Phys. Rev. B **54**, 14362 (1996).
[21] J. R. Chelikowsky, L. Kronik, I. Vasiliev, M. Jain, and Y. Saad, in *Handbook of Numerical Analysis Computational Chemistry*, edited by C. Le Bris (Elsevier, Amsterdam, 2003), Vol. X, pp. 613–637.
[22] Y. Zhou, Y. Saad, M. L. Tiago, and J. R. Chelikowsky, Phys. Rev. E **74**, 066704 (2006).
[23] J. R. Chelikowsky, M. L. Tiago, Y. Saad, and Y. Zhou, Comput. Phys. Commun. **177**, 1 (2007).
[24] M. M. G. Alemany, M. Jain, M. L. Tiago, Y. Zhou, Y. Saad, and J. R. Chelikowsky, Comput. Phys. Commun. **177**, 339 (2007); M. M. G. Alemany, R. C. Longo, L. J. Gallego, D. J. González,

L. E. González, M. L. Tiago, and J. R. Chelikowsky, Phys. Rev. B **76**, 214203 (2007).
[25] L. Collatz, *The Numerical Treatment of Differential Equations*, 3rd ed. (Springer-Verlag, Berlin, 1966), pp. 164, 389.
[26] J. L. Fattebert and J. Bernholc, Phys. Rev. B **62**, 1713 (2000); J.-L. Fattebert and F. Gygi, *ibid.* **73**, 115124 (2006).
[27] See, e.g., G. P. Srivastava, *Theoretical Modelling of Semiconductor Surfaces: Microscopic Studies of Electrons and Phonons* (World Scientific, Singapore, 1999); G. P. Srivastava, Rep. Prog. Phys. **60**, 561 (1997).
[28] J. Neugebauer and M. Scheffler, Phys. Rev. B **46**, 16067 (1992).
[29] G. Makov and M. C. Payne, Phys. Rev. B **51**, 4014 (1995).
[30] P. E. Blöchl, J. Chem. Phys. **103**, 7422 (1995).
[31] L. Bengtsson, Phys. Rev. B **59**, 12301 (1999).
[32] P. A. Schultz, Phys. Rev. B **60**, 1551 (1999).
[33] A. Natan, L. Kronik, and Y. Shapira, Appl. Surf. Sci. **252**, 7608 (2006).
[34] S. Ismail-Beigi, Phys. Rev. B **73**, 233103 (2006).
[35] I. Dabo, B. Kozinsky, N. E. Singh-Miller, and N. Marzari, Phys. Rev. B **77**, 115139 (2008).
[36] C. A. Rozzi, D. Varsano, A. Marini, E. K. U. Gross, and A. Rubio, Phys. Rev. B **73**, 205119 (2006).
[37] M. Otani and O. Sugino, Phys. Rev. B **73**, 115407 (2006).
[38] K. Hirose, T. Ono, Y. Fujimoto, and S. Tsukamoto, *First Principles Calculations in Real-Space Formalism* (Imperial College, London, 2005).
[39] A. Brandt and B. Diskin, SIAM J. Sci. Comput. (USA) **21**, 473 (1999).
[40] W. E. Pickett, Comput. Phys. Rep. **9**, 115 (1989).
[41] L. Kleinman and D. M. Bylander, Phys. Rev. Lett. **48**, 1425 (1982).
[42] The convergence of the total energy, Kohn-Sham eigenvalues, etc., is not necessarily dictated solely by the convergence of the kinetic energy term. For example, in Ref. 11 it is shown that, for oxygen, convergence is not aided by going above $N=4$, i.e., $O(h^8)$, in the finite-difference discretization. Our long-standing experience is that there is rarely anything to gain from going beyond $N=6$, i.e., $O(h^{12})$.
[43] Throughout this derivation we assume for simplicity that the grid spacing along $\hat{u}$ is equal to that along $\hat{v}$, i.e., $h_u=h_v$. If this is not the case, $\hat{u}\pm\hat{v}$ will generally not specify a grid point. In such a case one can still generate new directions compatible with grid points by defining $r=h_v/h_u$ and choosing a direction of the form $\hat{u}\pm r\cdot\hat{v}$. We have evaluated and implemented the more general formalism but for brevity present the more simple one.
[44] For a 2D non-Cartesian grid, $\partial/\partial\mu=(\hat{\mu}\cdot\hat{u})\partial/\partial u+(\hat{\mu}\cdot\hat{v})\partial/\partial v$, with an obvious generalization to a 3D grid.
[45] Note that $k_{uv}^{\pm}/2h_{uv}^2=f_{uv}|\hat{u}\pm v|^2/2h^2|\hat{u}\pm\hat{v}|^2=f_{uv}/2h^2$ so the discrete form can be further simplified by eliminating $k_{uv}^{\pm}$.
[46] For the lowest order of the discrete expansion, i.e., $N=1$ in Eq. (6), the discrete form of Eq. (21) reduces further to an expression identical to the so-called lattice Laplacian—see, e.g., Eq. (5) in V. Kobelev, A. B. Kolomeisky, and M. E. Fisher, J. Chem. Phys. **116**, 7589 (2002); or Eq. (4.41) in V. N. Astratov, A. M. Adawi, S. Fricker, M. S. Skolnick, D. M. Whittaker, and P. N. Pusey, Phys. Rev. B **66**, 165215 (2002).
[47] J. E. Lennard-Jones and M. Dent, Trans. Faraday Soc. **24**, 92 (1928).
[48] Alternatively, we could calculate the sum over the long-range component using Ewald-like methods. See Refs. 38 and 49.
[49] S. W. De Leeuw and J. W. Perram, Mol. Phys. **37**, 1313 (1979).
[50] www.nersc.gov/projects/paratec/
[51] N. Troullier and J. L. Martins, Phys. Rev. B **43**, 1993 (1991).
[52] Note that energy converges from above for plane waves, with increasing cutoff energy. However, it often converges from below for finite differences, with decreasing grid spacing. See P. Maragakis, J. M. Soler, and E. Kaxiras, Phys. Rev. B **64**, 193101 (2001).
[53] D. Naveh, L. Kronik, M. L. Tiago, and J. R. Chelikowsky, Phys. Rev. B **76**, 153407 (2007).
[54] S. Bei der Kellen and A. J. Freeman, Phys. Rev. B **54**, 11187 (1996).
[55] C. Filippi, D. J. Singh, and C. J. Umrigar, Phys. Rev. B **50**, 14947 (1994).
[56] G. Theurich and N. A. Hill, Phys. Rev. B **64**, 073106 (2001).
[57] L. Fernández-Seivane, M. A. Oliveira, S. Sanvito, and J. Ferrer, J. Phys.: Condens. Matter **18**, 7999 (2006).
[58] VASP calculations were performed using VASP 4.6 [G. Kresse and J. Furthmüller, Phys. Rev. B **54**, 11169 (1996)]; while treating the core electrons using the projector augmented wave method [G. Kresse, D. Joubert, *ibid.* **59**, 1758 (1999)].
[59] A. Natan, Y. Zidon, Y. Shapira, and L. Kronik, Phys. Rev. B **73**, 193310 (2006).